Supplementary Figures S1-12 and legends

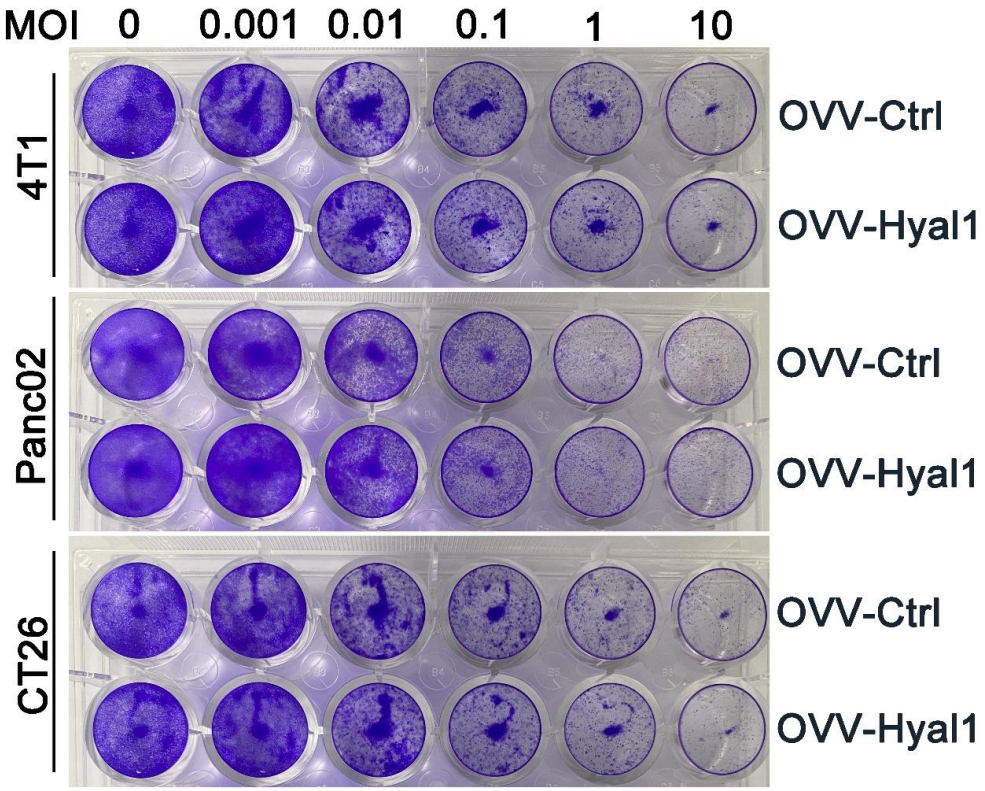

Figure S1. Comparison of the oncolysis between OVV-Hyal1 and OVV-Ctrl. 5×10^4 cells 4T1 breast cancer cells, Panc02 pancreatic carcinoma cells and CT26 colorectal cancer cells were seeded in 24-well plates. Then cells were treated with either OVV-Hyal1 or OVV-Ctrl at a serial of MOIs as depicted. 72 h later, cells were stained by crystal violet.

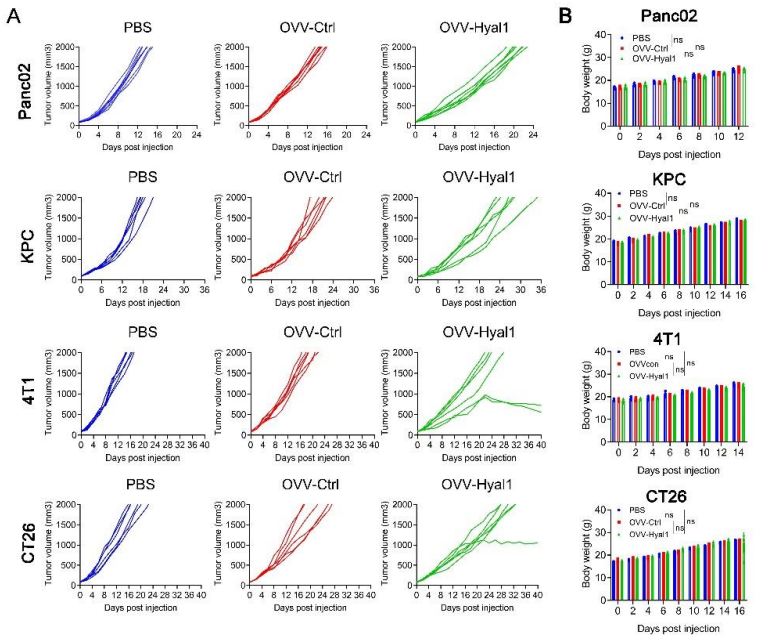

Figure S2. In vivo antitumor effects of OVV-Hyal1 and OVV-Ctrl. $5x10^5$ Panc02, $1x10^6$ KPC, $5x10^5$ 4T1 and $1x10^6$ CT26 were inoculated into the right flank of C57BL/6 or BALB/c mice. When tumor volume reached approximately 50 to 100 mm^3, mice were administered intratumorally (I.T.) with either $2x10^7$ pfu OVV-Hyal1 or OVV-Ctrl every other day for a total 3 times. Mice received PBS intratumoral injections were used as untreated controls. (A) The tumor volume was measured every two days until the volume exceeded 2000 mm^3. (B) Body weight of mice was measured every two days. Error bars represent SD. ns, not significant.

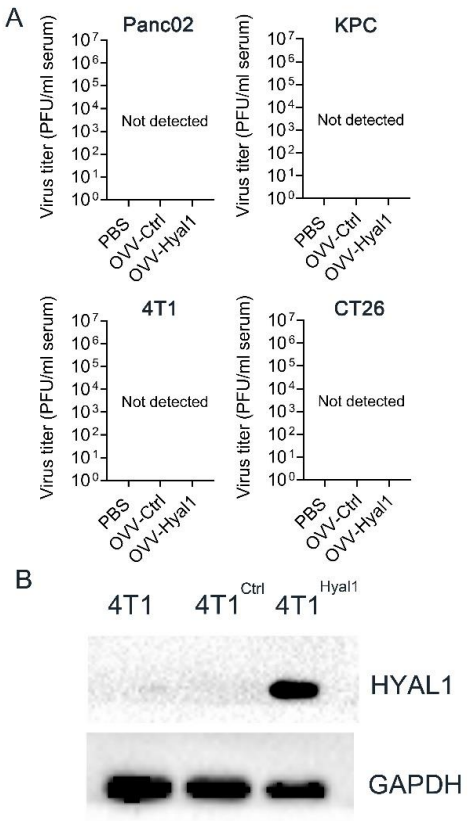

Figure S3. (A) The viral titers in the sera obtained from mice bearing Panc02, KPC, 4T1 and CT26, respectively, were quantified by TCID50 assay. (B) HYAL1 expression was determined in 4T1 cells stably expressing HYAL1 ($4T1^{Hyal1}$), or parental 4T1 cells by western blot.

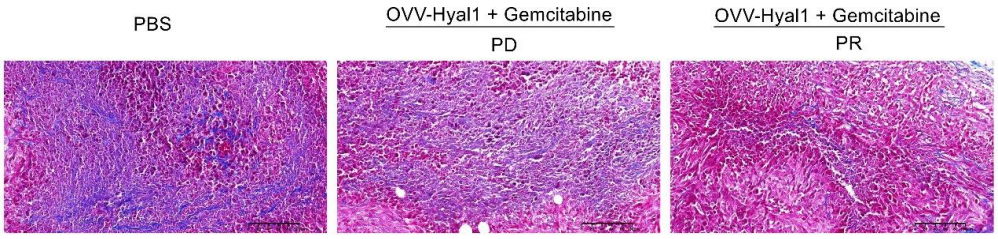

Figure S4. Differential degradation of ECM by OVV-Hyal1 in Panc02 tumors. Subcutaneous Panc02 tumors were treated with OVV-Hyal1 and gemcitabine. Then tumor tissue were obtained 30 days after the treatment from the mice with either partial remission (PR) or progressive disease (PD), respectively. Masson staining was

used to analyze the ECM degradation. Collagen was stained in blue. Scale bars are equal to 100 μm.

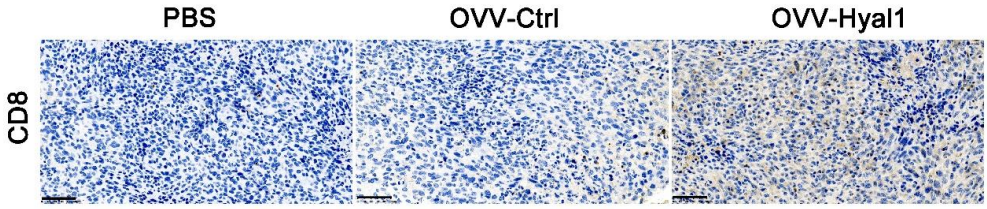

Figure S5. Immunohistochemistry for CD8 in Panc02 model. $5x10^5$ Panc02 were inoculated into the right flank of C57BL/6 mice. When tumor volume reached approximately 50 to 100 mm^3, mice were administered intratumorally (I.T.) with either $2x10^7$ pfu OVV-Hyal1 or OVV-Ctrl every other day for a total 3 times. Mice received PBS intratumoral injections were used as untreated controls. Tumor tissue were obtained 2 days after last viral injection, and infiltration of $CD8^+$ T cells in tTME was determined by immunohistochemical staining. Scale bar are equal to 50 μm.

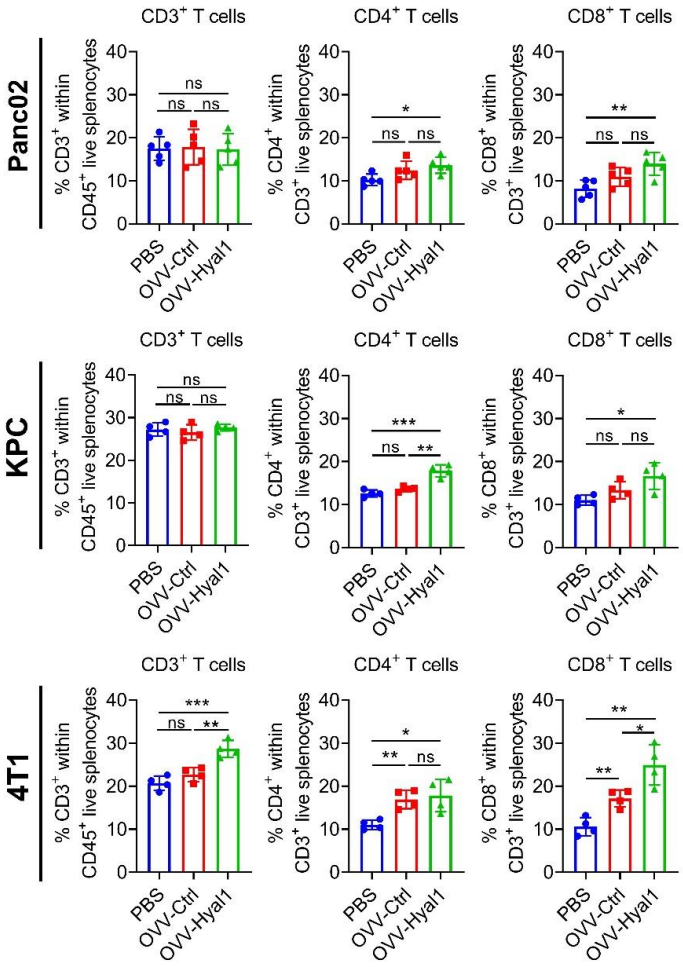

Figure S6. Flow cytometric analysis of the proportion of $CD3^+$, $CD8^+$ and $CD4^+$ T cells in splenocytes. Panc02, KPC and 4T1 models were established as previously described in Figure 1E and the single-cell suspensions were preprepared two days after last viral injection. Error bars represent SD. ns, not significant; *p<0.05; **p<0.01; ***p<0.001.

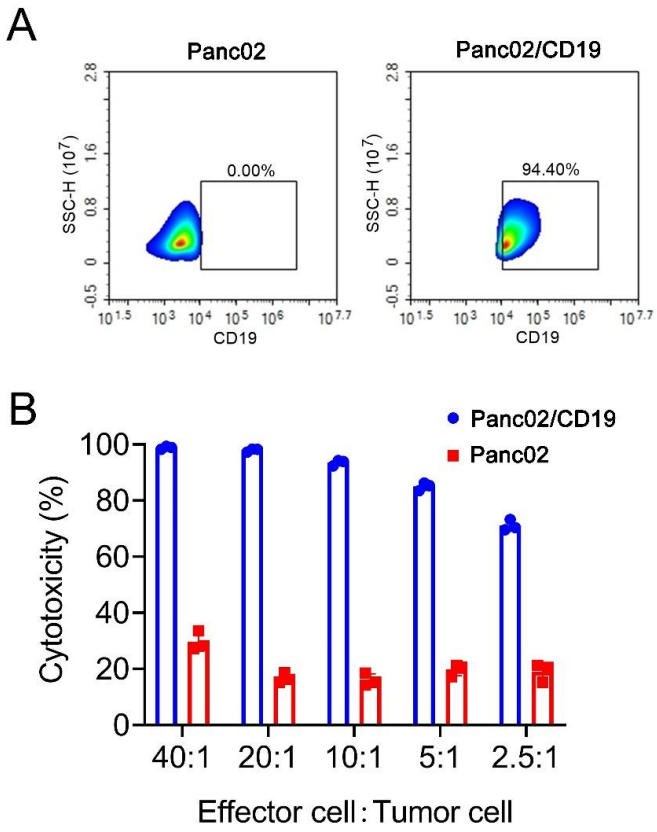

Figure S7. Characterization of Panc02/CD19 cells. (A) Panc-02/CD19 cell line was stably expressed the human CD19 antigen, which was detected by flow cytometry. (B) Panc-02/CD19 served as the tumor target of CD19 CAR-T cells. The CD19-CAR-T cells were co-cultured with Panc02/CD19 or parental panc-02 cells with luciferase reporter gene in round bottom 96-well-plates at different ET ratios for 24 h. Error bars represent SD.

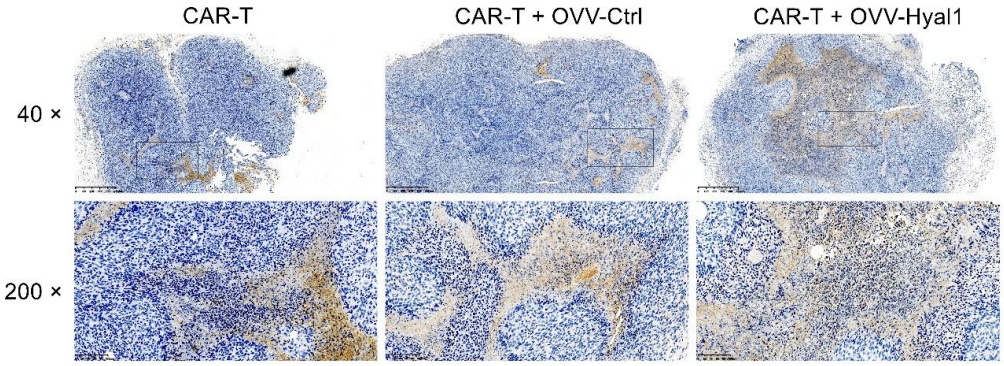

Figure S8. Distribution of CD19 CAR-T cells in the tumor tissue in Panc02/CD19 subcutaneous model. The establishment of the Panc02/CD19 model and the treatment scheme have been shown in Figure 4D. Immunohistochemistry in Panc02 model. Immunohistochemical staining for FMC63 scFv (brown staining) was used to detect the infiltration of CD19 CAR-T cells in the tumor tissue. Scale bars are equal to 625 μm (upper panel) and 100 μm (lower panel), respectively.

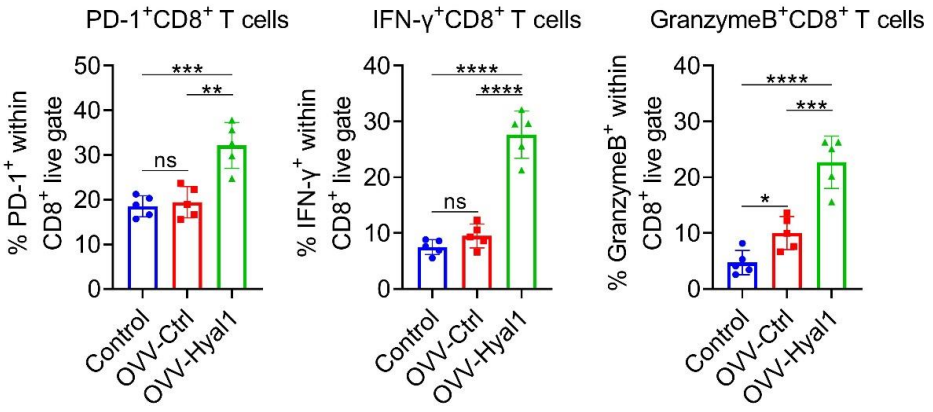

Figure S9. Immune activation status of $CD8^+$ T cells after treatment. 4T1 models were established as previously described in Figure 1E, single cell suspensions were preprepared two days after last viral injection and subjected to flow cytometry to analyze the PD-1, IFN-γ and Granzyme B expression on $CD8^+$ T cells. Error bars represent SD. ns, not significant; **p < 0.01; *** p < 0.001; **** p < 0.0001.

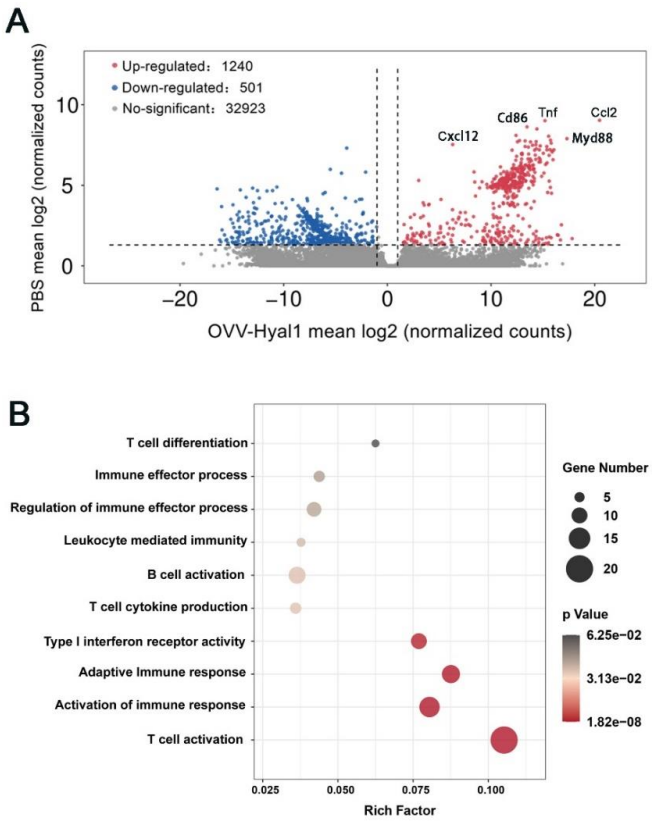

Figure S10. Gene expression in the TME by RNA-seq analysis. (A) Tumors treated with OVV-Hyal1 for 10 days were harvested, and gene expression analysis was performed using RNA-seq. The differential gene expression between the samples treated with OVV-Hyal1 and PBS, using the absolute value of logFC greater than 1 as the threshold. (B) Top 10 gene ontology enrichment terms of DEGs. Bar size indicates the number of DEGs in that gene class, and the color reflects the p value of the enriched term. The p value is higher from red to black.

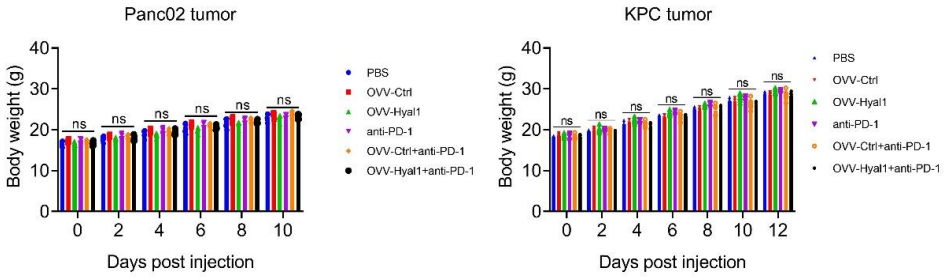

Figure S11. Body weight monitoring during therapy. Mice body weight were observed in Panc02 (A) and KPC (B) pancreatic subcutaneous tumor model treated with combined therapy of OVV-Hyal1 and anti-PD-1 antibody. Error bars represent SD. ns, not significant.

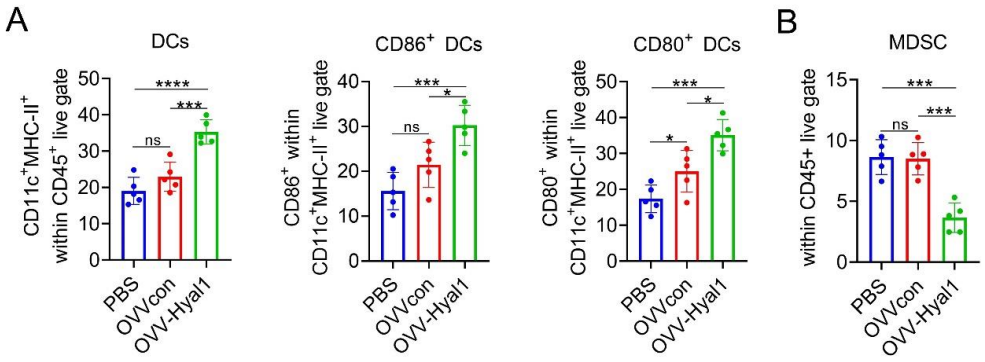

Figure S12. OVV-Hyal1 significantly increased the infiltration of DCs and their activity in pancreatic carcinoma. Panc02 models were established as previously described in Figure 1E and the single-cell suspensions were preprepared two days after last viral injection. (A) Flow cytometric analysis of the proportions of $CD11c^+$ MHC class II^+ dendritic cells in $CD45^+$ cells, $CD86^+$ or $CD80^+$ mature dendritic cells in $CD45^+$ $CD11c^+$ MHC class II^+ cells in Panc02 tumors. (B) Flow cytometric analysis of the proportions of $CD11b^+$ $Gr\text{-}1^+$ MDSC cells in $CD45^+$ cells in Panc02 tumors. Error bars represent SD. ns, not significant; * $p < 0.05$; *** $p < 0.001$; **** $p < 0.0001$.